Published OnlineFirst June 26, 2017; DOI: 10.1158/0008-5472.CAN-17-0657

Microenvironment and Immunology

Cancer Research

SPIN90 Depletion and Microtubule Acetylation Mediate Stromal Fibroblast Activation in Breast Cancer Progression

Eunae You[1], Yun Hyun Huh[2], Ahreum Kwon[2], So Hee Kim[2], In Hee Chae[2], Ok-Jun Lee[3], Je-Hwang Ryu[4], Min Ho Park[5], Ga-Eon Kim[6], Ji Shin Lee[6], Kun Ho Lee[7], Yong-Seok Lee[1], Jung-Woong Kim[1], Sangmyung Rhee[1], and Woo Keun Song[2]

Abstract

Biomechanical remodeling of stroma by cancer-associated fibroblasts (CAF) in early stages of cancer is critical for cancer progression, and mechanical cues such as extracellular matrix stiffness control cell differentiation and malignant progression. However, the mechanism by which CAF activation occurs in low stiffness stroma in early stages of cancer is unclear. Here, we investigated the molecular mechanism underlying CAF regulation by SPIN90 and microtubule acetylation under conditions of mechanically soft matrices corresponding to normal stromal rigidity. SPIN90 was downregulated in breast cancer stroma but not tumor, and this low stromal expression correlated with decreased survival in breast cancer patients. *Spin90* deficiency facilitated recruitment of mDia2 and APC complex to microtubules, resulting in increased microtubule acetylation. This increased acetylation promoted nuclear localization of YAP, which upregulated expression of myofibroblast marker genes on soft matrices. *Spin90* depletion enhanced tumor progression, and blockade of microtubule acetylation in CAF significantly inhibited tumor growth in mice. Together, our data demonstrate that loss of SPIN90-mediated microtubule acetylation is a key step in CAF activation in low stiffness stroma. Moreover, correlation among these factors in human breast cancer tissue supports the clinical relevance of SPIN90 and microtubule acetylation in tumor development. *Cancer Res; 77(17); 4710–22. ©2017 AACR.*

Introduction

Interactions between cancer cells and their surrounding stroma are critical for cancer progression. Normal stromal cells inhibit tumorigenicity. However, tumor conditions surmount inhibitory activity of stromal cells at a critical point and induce changes that facilitate cancer progression (1). During early tumor development, quiescent fibroblasts, the predominant cell type within normal stroma, undergo transition into myofibroblast-like cells, known as cancer-associated fibroblasts (CAF). CAFs are responsible for extracellular matrix (ECM) biosynthesis and mechanical remodeling of cancer stroma. Changes in cancer stroma induced by CAF activation lead to the development of a permissive environment for tumor growth and metastasis. For instance, stiff ECM created by CAF-mediated collagen crosslinking promotes malignancy in breast tumors (2), while reduction in cell tension suppresses the malignant behavior of mammary epithelial cells (3). During tumorigenesis, dense deposition of stromal ECM by primed stromal fibroblasts and surrounding cancer cells results in increased stiffness, in turn, inducing the expression of myofibroblast-specific genes, such as α-smooth muscle actin (α-SMA) and fibroblast activation protein (4).

CAFs acquire an activated phenotype with enhanced expression of α-SMA, increased cell contractility and spindle shape resembling myofibroblast phenotypes commonly observed in wounds (5). CAF activation occurs in the stroma during the early stage of breast cancer where tissue stiffness is relatively low (6). In a two-dimensional (2D) culture system mimicking stiff matrix conditions, myofibroblast differentiation has been well established (7). In particular, TGFβ–induced myofibroblast differentiation requires cell adhesion and integrin signaling (7), which mediates the acquisition of actomyosin-mediated cellular contractility and adhesion. However, in a soft three-dimensional (3D) matrix mimicking normal tissue stroma, fibroblasts lack integrin- and actin-dependent focal adhesion (8, 9).

The observed cell properties on a 3D soft matrix suggest that microtubules are responsible for mechanical sensing of soft matrix. Human fibroblasts cultured in relaxed 3D collagen matrices exhibit neuron-like dendritic extensions with microtubule

[1]Department of Life Science, Chung-Ang University, Seoul, Republic of Korea. [2]Bio Imaging and Cell Logistics Research Center, School of Life Sciences, Gwangju Institute of Science and Technology, Gwangju, Republic of Korea. [3]Department of Pathology, Chungbuk National University College of Medicine, Chungdae-ro 1, Seowon-Gu, Cheongju, Republic of Korea. [4]Dental Science Research Institute and Research Center for Biomineralization Disorders, School of Dentistry, Chonnam National University, Gwangju, Republic of Korea. [5]Department of Surgery, Chonnam National University Medical School, Gwangju, Republic of Korea. [6]Department of Pathology, Chonnam National University Hwasun Hospital, Hwasun, Republic of Korea. [7]Department of Biomedical Science and National Research Center for Dementia, Chosun University, Gwangju, Republic of Korea

Note: Supplementary data for this article are available at Cancer Research Online (http://cancerres.aacrjournals.org/).

E. You and Y.H. Huh contributed equally to this article.

Corresponding Authors: Woo Keun Song, Gwangju Institute of Science and Technology, 123 Cheomdan Gwagi-ro, Buk-Gu, Gwangju, 61005, Republic of Korea. Phone: 82-62-715-2487; Fax: 82-62-715-2543; E-mail: wksong@gist.ac.kr; and Sangmyung Rhee, Chung-Ang University, Seoul, 06974, Republic of Korea, Phone: 82-2-820-5818; Fax: 82-2-825-5206; E-mail: sangmyung.rhee@cau.ac.kr

doi: 10.1158/0008-5472.CAN-17-0657

Published OnlineFirst June 26, 2017; DOI: 10.1158/0008-5472.CAN-17-0657

core and actin-rich tips lacking integrin-mediated focal adhesions (10), indicating that cell–matrix interactions in soft matrix environments are different from those in stiff matrices. Earlier reports suggest that microtubule predominantly participates in cellular contractility and force generation under 3D soft environments (11, 12). In support of these findings, myosin IIA-deficient fibroblasts have been shown to develop low-tension interactions with soft matrix containing prominent bundles of stabilized microtubules (13). Interestingly, increased acetylation of α-tubulin at lysine 40 (K40) was recently reported in metastatic breast cancer cells (14). Moreover, high HDAC6 and low acetylated α-tubulin levels are associated with good prognosis in breast cancer (15). These findings highlight the physiologic relevance of tubulin acetylation in cancer progression. Additionally, elucidation of the mechanisms leading to CAF activation in stroma with low stiffness during the early stage of cancer is necessary to gain insights into cancer progression.

Yes-associated protein 1 (YAP), originally identified as a transcriptional coregulator of the Hippo pathway, has emerged as an important player in mechanotransduction. The subcellular localization and activity of YAP are regulated by substrate stiffness (16–19) and its activation in CAFs promotes stiffening of ECM through extensive deposition of collagen (20). The stiffened matrix, in turn, creates tension within CAFs, leading to nuclear translocation of YAP and expression of genes encoding cytoskeletal regulators, such as ANLN and CTGF (16).

In this study, we demonstrated significant downregulation of SPIN90 (Src homology 3 protein interacting with NCK, 90 kDa) in breast cancer stroma with a concomitant increase in microtubule acetylation and YAP activation. These results establish the mechanism underlying CAF differentiation in low stiffness of stromal environment of early stage breast cancer.

Materials and Methods

Human cancer tissues and experimental mouse model

Human breast cancer tissues were kindly provided and analyzed by Chungbuk National University Hospital of the Korea Biobank Network, and tissue microarray of breast cancer tissues (diagnosed in 2008–2009) were provided by Chonnam National University Hospital of Korea Biobank Network (20160120-BR-21-03-02). Written informed consents were obtained from the patients before surgery and this study was approved by the Gwangju Institute of Science and Technology (GIST) Institutional Review Board. *Spin90*$^{-/-}$ mice were generated by inserting a pgk-neomycin cassette into the NheI site of exon 4. All animal procedures were performed with the approval of the Animal Care and Ethics Committees of the GIST (GIST-2014-09).

Cell lines

Mouse embryonic fibroblasts (MEF) were isolated from embryos at 12.5 days postcoitum. The SV40 large T-antigen was transfected into MEFs for immortalization in 2008. MEF cells were authenticated by morphologic profiling and genotyping and RT-PCR in 2013. E0771, mouse medullary mammary adenocarcinoma cells derived from C57/BL6 mice were purchased from CH3 Biosystems and authenticated by morphologic profiling in 2015. Primary CAFs were isolated from mammary tumors of wild-type (WT) and *Spin90*$^{-/-}$ mice using flow cytometry and authenticated by RT-PCR in 2015. Every cell line usually used from passages 3 to 8. All cell lines were tested for Mycoplasma contamination using the MycoAlert mycoplasma detection Kit (Lonza) in 2015.

Polyacrylamide gels preparation

Polyacrylamide gels (PAG) varying in stiffness from 0.5 to 20 kPa were prepared as previously described (10, 21). The activated PAGs were coated with 10 μg/mL human plasma fibronectin (FN; Gibco) overnight at 4°C. Stiffness was measured by atomic force microscopy.

RT-PCR

Total RNA was prepared using TRI reagent (Molecular Research Center, Cincinnati, OH) and reverse-transcribed by TOPscript RT DryMIX (Enzynomics). cDNA was subjected to PCR using Taq polymerase (iNtRON BioTechnology) with primers (Supplementary Table S1).

3D collagen gel contraction assay

A total of 2×10^5 cells were mixed with collagen (1 mg/mL) and FN (100 μg/mL) solution and polymerized for 1 hour. Floating matrix contraction (FMC) and stressed matrix contraction (SMC) were measured as described (22).

Modified Boyden chamber assay

Conditioned media (CM) derived from MEFs were prepared by incubation for 36 hours in serum-free DMEM. MDA-MB-231 cells were seeded on 300 μg/mL Matrigel (BD Biosciences) coated or uncoated transwells with 8.0-μm pores (Corning Costar), and CM was added to the lower chamber. After 24-hour incubation, cells were fixed and stained with 0.05% Crystal violet in 2% EtOH. Cells that invaded the bottom layer of transwell inserts were counted in nine randomly selected fields.

In vivo-like organotypic culture

Collagen gel preparation was done as described previously (23). MEFs were suspended in collagen gel solution and mixtures were polymerized at 37°C. After polymerization, MDA-MB-231 (2.5×10^5 cells) were seeded on collagen gels. After 2 weeks, gels were standard hematoxylin and eosin staining of paraffin sections. Invading cells were quantified by MetaMorph software (Molecular Devices) and the invasion index was measured by the following formula: [1−(noninvading area/total area)].

Orthotopic breast cancer model

Congenic female C57/BL6-*Spin90*$^{-/-}$ or WT mice (10–14-week-old) were used for the orthotopic breast cancer model. E0771 (5×10^5 cells) suspended in PBS were inoculated into the left inguinal mammary fat pad. Tumor size was measured daily using calipers, and tumor volume (V) was calculated using the standard method, $V = (L \times W^2)/2$, where W is width, and L is length. After 4 weeks, tumors and lungs were isolated.

Immunohistochemistry

Mammary tumors and lungs were excised from mice and fixed in 10% formalin or Bouin's solution and embedded in paraffin blocks. Sectioned tissues were stained with specific antibodies such as anti-mouse SPIN90 for human tissues (clone 84B3), anti-rabbit SPIN90 for mouse tissues (Proteintech), α-SMA, acetylated α-tubulin, and YAP. Nuclei were counterstained with hematoxylin or Hoechst 33342. Colorimetric analysis was performed

Published OnlineFirst June 26, 2017; DOI: 10.1158/0008-5472.CAN-17-0657

using an Aperio Image Scope (Leica Biosystems) and Image J software. Colorimetric analyses were performed using an Aperio Image Scope (Leica Biosystems) and ImageJ software. To analyze correlations between SPIN90 expression and α-tubulin acetylation in human breast cancer tissues, we measured the total intensity of positive pixels per observed area in five randomly selected areas of paired normal and cancer stroma using the Positive Pixel Counts v.9.1 algorithm. The intensity in tumor stroma (I.T.) relative to the intensity in normal stroma (I.N.), calculated as the log of the ratio, I.T./I.N., in base 2 [Log_2(I.T./I.N.)], was evaluated to determine Pearson correlation coefficient (r) and the statistical significance of r (P value) using a t test. An absolute value of Log_2(I.T./I.N.) greater than 1 indicates at least a two-fold increase or decrease in tumor stroma compared with normal stroma. Fluorescence staining in tissues was detected by confocal microscopy (Olympus FV1000) and analyzed with MetaMorph software.

Statistical analysis

Quantitative human tissue immunochemistry results and public transcriptome data were analyzed using a Pearson correlation test and false discovery rate-adjusted P value (q), respectively. All quantified data in bar charts are shown as means ± SEM, and represent an average of 3 to 4 independent experiments. Data in box and whisker plots and scattered plots represent differences between populations. A two-tailed Student t test with unequal variance was used for comparison of parameters between two groups. All P values are two-sided. Data were considered

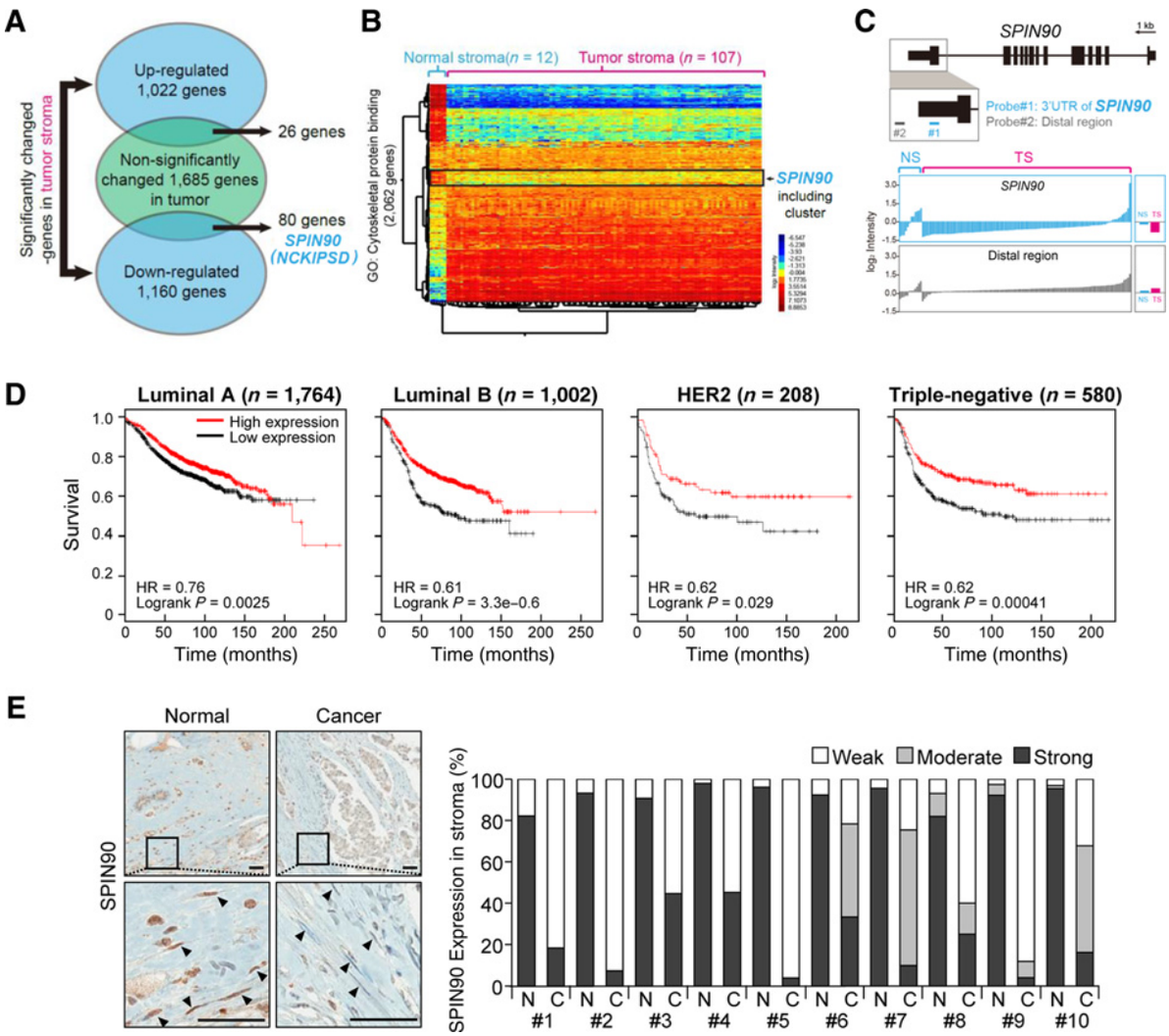

Figure 1.

Low SPIN90 expression is correlated with poor prognosis in breast cancer patients. **A** and **B,** Analysis of the combined gene expression datasets GSE39004 and GSE9014. Stroma-specific downregulated or upregulated genes were functionally annotated based on gene ontology term analyses. **C,** Two set probes recognizing *SPIN90*. Probe #1 binds to the 3′-UTR and probe #2 recognizes the distal region of *SPIN90*. **D,** KM survival curves of human breast cancer patients expressing low levels of *SPIN90*, compared with patients with high *SPIN90* expression. All 3554 patients were divided into four molecular subgroups for analysis: luminal A ($n = 1764$), luminal B ($n = 1002$), HER2 type ($n = 208$), and triple-negative (TN; $n = 580$). **E,** Downregulation of SPIN90 in breast cancer tissues, compared with paired normal tissues ($n = 10$). Scale bar, 50 μm.

Published OnlineFirst June 26, 2017; DOI: 10.1158/0008-5472.CAN-17-0657

statistically significant at *P* values less than 0.05; *, $P \leq 0.05$; **, $P \leq 0.01$; ***, $P \leq 0.001$.

Results

Clinical relevance of SPIN90 downregulation in CAFs

We analyzed public transcriptome data, with the goal of identifying the specific regulators of CAF activation in breast cancer stroma. To screen differentially expressed genes between normal and cancer stroma that were not significantly changed in tumors, 1,685 genes (unchanged in tumor, compared with normal tissue) were initially sorted ($n = 50$, *P* value > 0.5; PMID: 24316975, GSE39004; Supplementary Fig. S1A and S1B). Among these, 26 upregulated (*P* value < 0.05) and 80 downregulated (*P* value < 0.05) genes in cancer stroma were selected (PMID: 18438415, GSE9014; Fig. 1A). In the tumor microenvironment, ECM composition and stromal stiffness depend on the activation state of fibroblasts. Morphologic differences between normal stromal fibroblasts and activated CAFs, including spreading and elongation, were significant. We, thus, focused on the gene set involved in "cytoskeletal protein binding" (GO: 0008092). Intersection of 106 differentially regulated genes in the cancer stroma with 2,062 genes annotated to the term "cytoskeletal protein binding" led to the isolation of five genes (*NCKIPSD*, *LZTS1*, *TPM1*, *EMD*, and *TPM3*), of which *SPIN90* (*NCKIPSD*) was selected for examination as a potential regulator of CAF activation based on the Kaplan–Meier (KM) plot analysis (Supplementary Fig. S1C). Downregulation of *SPIN90* in cancer stroma ($n = 107$), compared with normal stroma ($n = 12$), was confirmed via GO term analysis of the gene set "cytoskeletal protein binding" (Fig. 1B, fold change > 2; FDR < 1%). *SPIN90* mRNA expression in breast cancer stroma was validated using two sets of probes, one that recognizes the 3′UTR, which is more specific for targeting *SPIN90*, and one that recognizes the distal region, which is less specific. Using the 3′UTR probe, but not the distal probe, we observed a distinct decrease in *SPIN90* transcript expression in breast cancer stroma (Fig. 1C; Supplementary Fig. S1D).

For the clinical relevance of *SPIN90* downregulation in breast cancer stroma, we used KM plot analysis based on a human gene expression-array database (Affymetrix ID: 216116 on www.kmplot.com/analysis). Decreased survival of patients with low levels of *SPIN90* mRNA was observed for all molecular subtypes of breast cancer, including luminal A ($n = 1764$), luminal B ($n = 1002$), HER2-type ($n = 208$), and triple-negative ($n = 580$) groups (Fig. 1D). Histologic analyses of paired normal and breast cancer

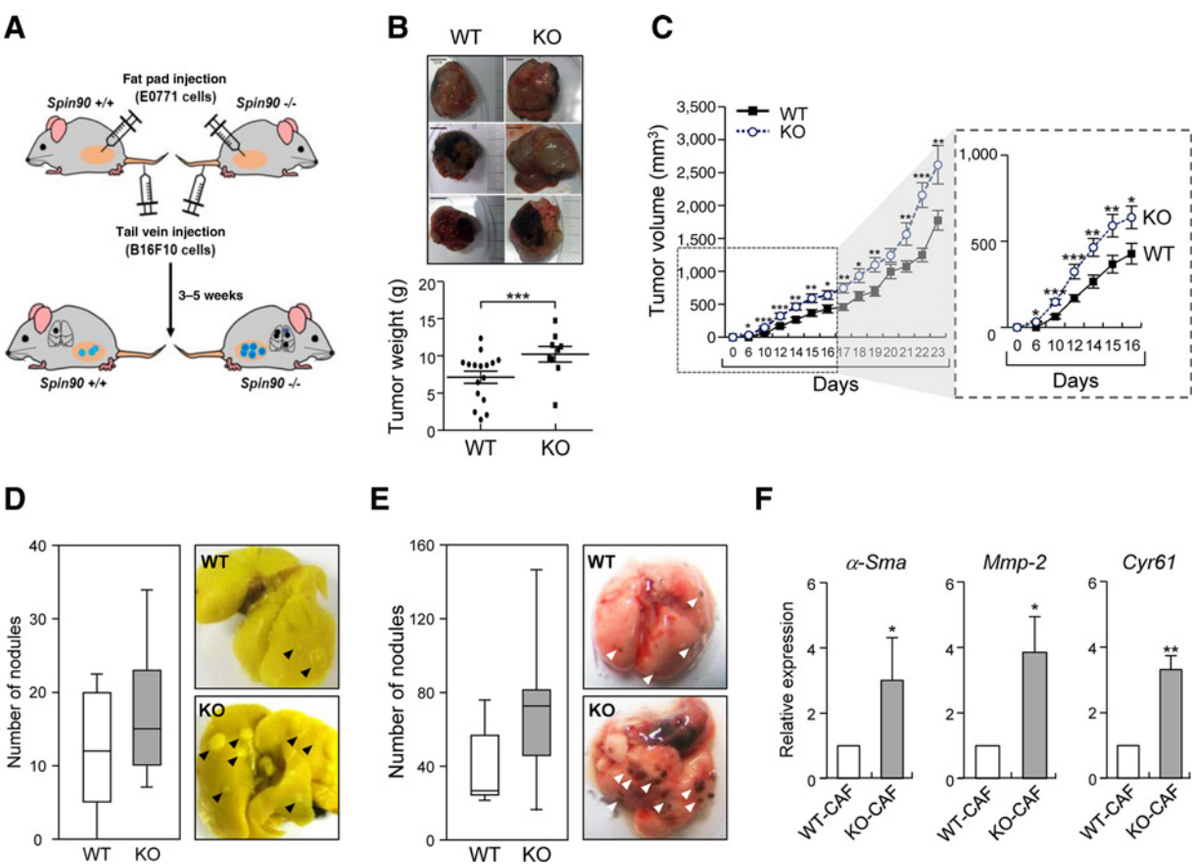

Figure 2.

Cancer progression is accelerated in *Spin90*$^{-/-}$ mice. **A,** Scheme of the experimental procedure. **B–D,** Orthotopic injection of E0771 cells into mammary fat pads of syngeneic WT ($n = 15$) and *Spin90*$^{-/-}$ mice ($n = 9$), and comparison of tumor weights and representative images (**B**). Tumors were allowed to grow for 23 days. Graphs depict tumor volumes over time (**C**). *, $P < 0.05$; **, $P < 0.01$. Lungs were fixed with Bouin's solution and analyzed for metastasis (**D**). **E,** Lung metastasis model of intravein-injected B16F10 melanoma cells. **F,** CAF marker expression by qPCR in CAFs isolated from the E0771-injected murine model. *, $P \leq 0.05$; **, $P \leq 0.01$; ***, $P \leq 0.001$.

Published OnlineFirst June 26, 2017; DOI: 10.1158/0008-5472.CAN-17-0657

tissues ($n = 10$) revealed dramatic downregulation of SPIN90 in CAFs of cancer stroma, but not in cancer cells and immune cells (Fig. 1E; Supplementary Fig. S1E). Data mining using public GEO data analysis in ovarian cancer (GSE40595) further confirmed reduced expression of *SPIN90* in CAFs (Supplementary Fig. S1F). Interestingly, downregulation of *SPIN90* in CAFs of lung metastases (CAF-LM) was more pronounced than that in fibroblasts of primary colorectal tumor (CAF-PT; GSE46824; Supplementary Fig. S1G).

To ascertain whether SPIN90 deficiency is relevant to tumorigenesis and metastasis, we performed orthotopic injection of syngeneic murine breast cancer cells, E0771, into mammary fat pads or intravein injection of syngeneic melanoma cells, B16F10, into the tail veins of WT and *Spin90*$^{-/-}$ [knockout (KO)] mice (Fig. 2A). The resulting tumors were bigger in mammary glands of *Spin90*$^{-/-}$ mice, compared with those of WT mice, and interestingly, a prominent increase in tumor volume in *Spin90*$^{-/-}$ mice was observed during initial tumor growth (Fig. 2B and C). Moreover, all *Spin90*$^{-/-}$ mice ($n = 9$) bearing E0771 breast tumors developed lung metastasis whereas 20% WT mice ($n = 15$) remained metastasis-free and the rest displayed fewer metastatic nodules (Fig. 2D; Supplementary Fig. S2A). Injection of B16F10 melanoma cells also induced increased lung metastasis in *Spin90*$^{-/-}$ mice (Fig. 2E; Supplementary Fig. S2B), indicating that SPIN90 deficiency in the stroma facilitates favorable conditions for cancer progression. To compare the activation states of CAFs in

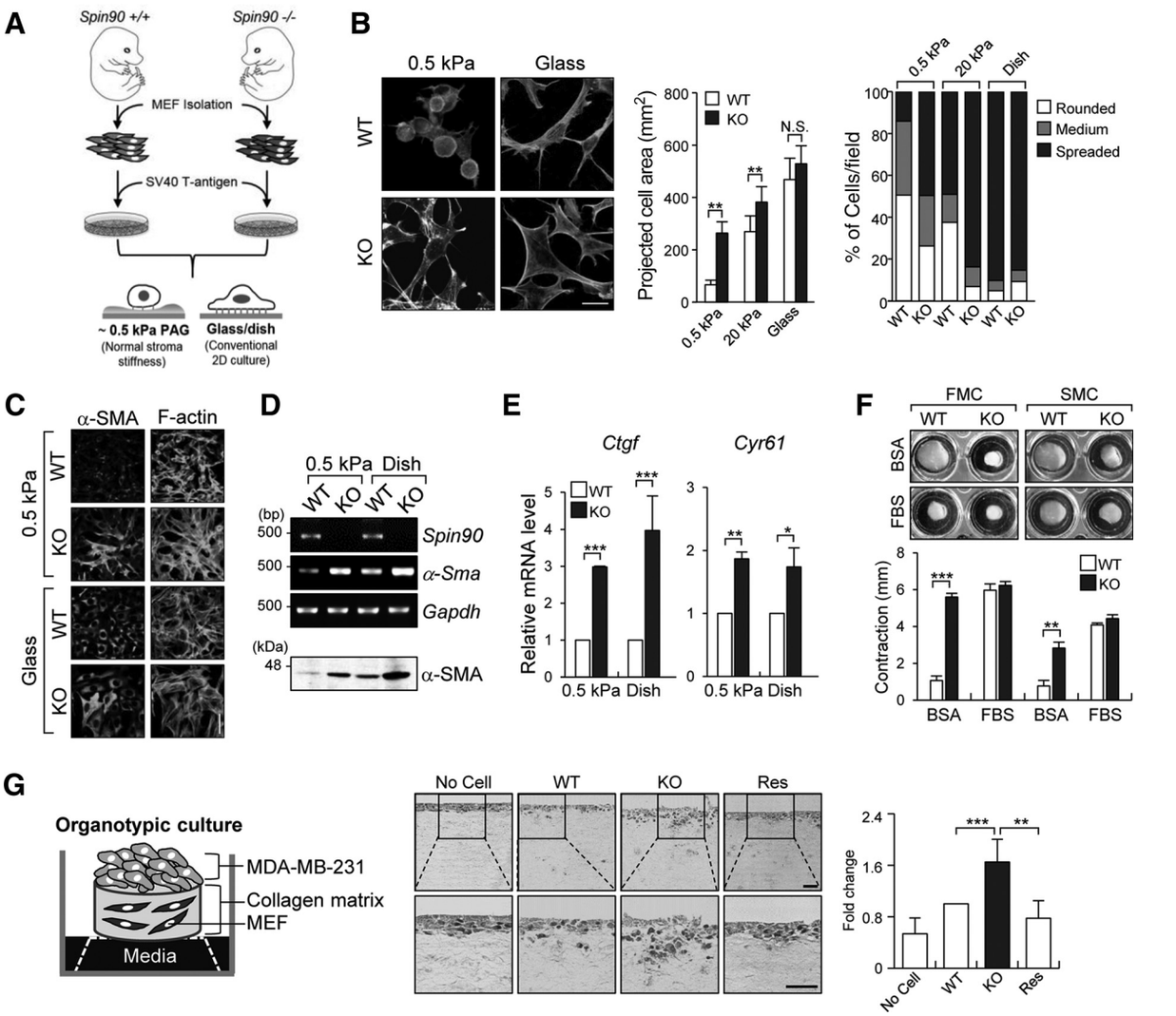

Figure 3.

Isolated *Spin90*-KO MEFs possess CAF characteristics. **A,** Schematic overview of MEF isolation and experimental conditions. **B–E,** WT and *Spin90*-KO MEFs were seeded on fibronectin-coated 0.5 kPa PAG or glass. **B,** Projected cell area and percentage/field with morphologic index (round, medium, well-spread) were measured. Scale bar, 20 μm. **C,** Cells were stained with α-SMA antibody and phalloidin to visualize F-actin. Scale bar, 50 μm. **D,** RT-PCR of *Spin90, α-Sma* and *Gapdh* and immunoblotting of α-SMA. **E,** qPCR analysis of *Ctgf* and *Cyr61.* Graphs depict relative expression normalized to *Gapdh*. **F,** Matrices were floated for 12 hours with BSA (5 mg/mL) or FBS (FMC), or attached for 18 hours, then released from the bottom and incubated for 1 hour (SMC). **G,** Illustration of organotypic culture and hematoxylin and eosin–stained sections of MDA-MB-231 cells cultured on organotypic gels in the absence or presence of WT, *Spin90*-KO, and rescued MEFs. Scale bar, 50 μm. *, $P \leq 0.05$; **, $P \leq 0.01$; ***, $P \leq 0.001$. N.S., nonsignificant.

Published OnlineFirst June 26, 2017; DOI: 10.1158/0008-5472.CAN-17-0657

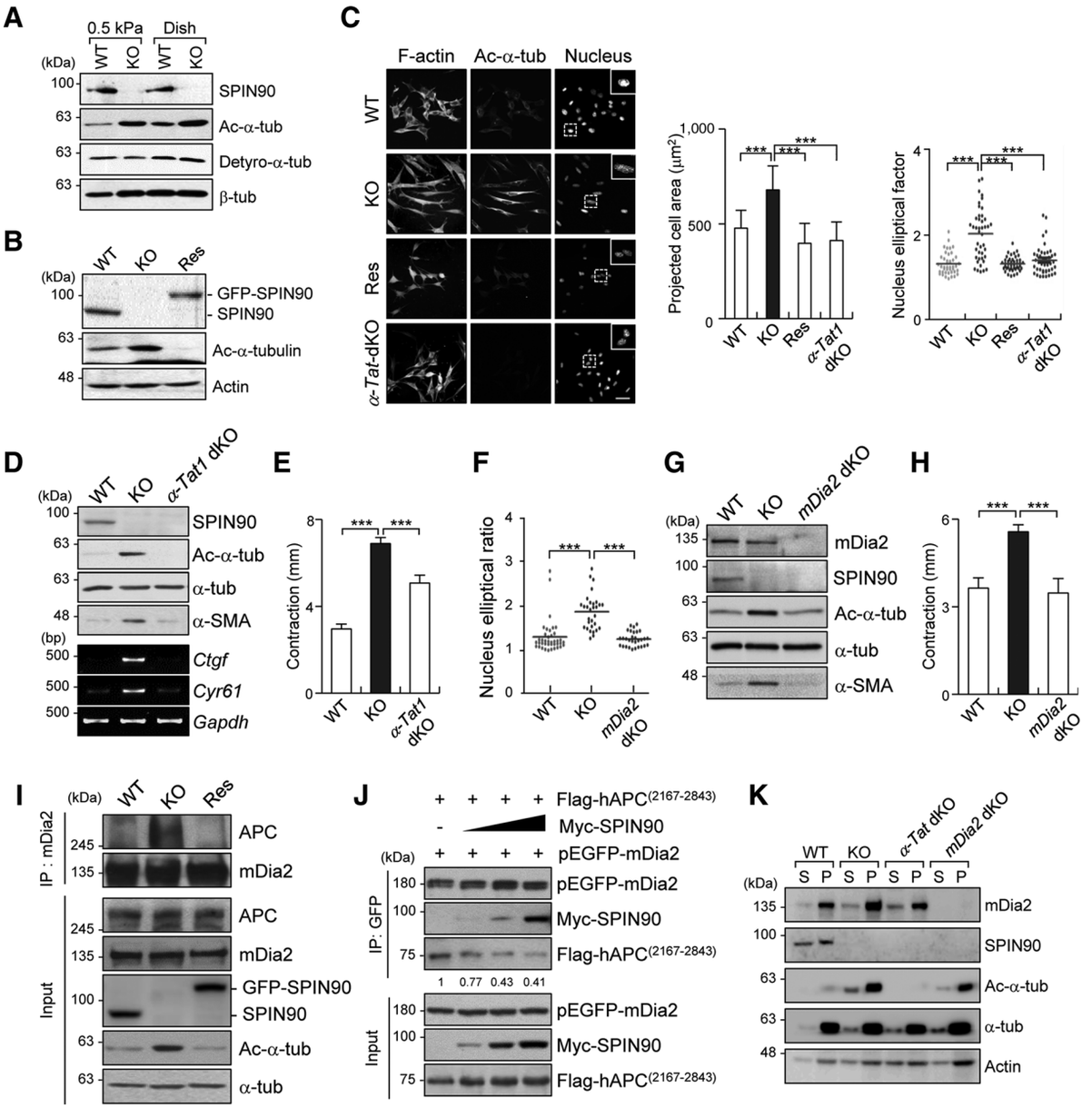

Figure 4.

Microtubule acetylation is critical for myofibroblast differentiation. **A** and **B,** Cell lysates obtained from WT, *Spin90*-KO (**A**), and *Spin90*-rescued MEFs (**B**) were subjected to immunoblotting with acetylated α-tubulin and detyrosinated α-tubulin antibodies. **C,** Morphologic analysis of WT, *Spin90*-KO, *Spin90*-rescued, and *α-Tat1*-dKO cells on 0.5 kPa PAGs. Cells were analyzed for projected cell area and nucleus elliptical factor. ***, $P < 0.001$. **D** and **E,** Inhibition of α-tubulin acetylation via *α-Tat1* knockout decreases α-SMA expression (**D**) and cellular contractility (for 12 hours) in *Spin90*-KO MEFs (**E**). **F,** Nuclear elliptical ratio of WT, *Spin90*-KO, and *mDia2*-dKO MEFs. ***, $P < 0.001$. **G** and **H,** Loss of *mDia2* in *Spin90*-KO MEFs inhibits α-SMA expression (**G**) and contractility (**H**). ***, $P < 0.001$. **I,** Immunoprecipitation with an anti-mDia2 antibody. **J,** HEK293T cells were transfected with Flag-APC, pEGFP-mDia2, and myc-SPIN90 (0, 125, 250, and 500 ng) and applied for immunoprecipitation. **K,** Cells on 0.5 kPa gels were lysed with hypotonic buffer containing cytochalasin D and paclitaxel and centrifuged 100,000 × *g*.

stroma of WT and *Spin90*$^{-/-}$ mice, we isolated stromal fibroblasts from tumors of both groups (Supplementary Fig. S2C) via fluorescence-activated cell sorting using an anti-PDGFR^{+}α antibody (Supplementary Fig. S2D). The purity of the sorted CAF population was verified via qPCR analysis of genes specific for fibroblasts (*Pdgfrα*), macrophages (*Csf-1r*), and lymphocytes (*Cd45*; Supplementary Fig. S2E). Fibroblasts originating from *Spin90*$^{-/-}$ mice showed a more activated phenotype than those from WT mice, determined based on increased expression of *α-Sma, Mmp-2,* and *Cyr61* (Fig. 2F).

Loss of SPIN90 induces myofibroblast differentiation

As the rigidity of stroma in the early stages of cancer is similar to that of normal stroma, we compared the morphology of MEFs on

Published OnlineFirst June 26, 2017; DOI: 10.1158/0008-5472.CAN-17-0657

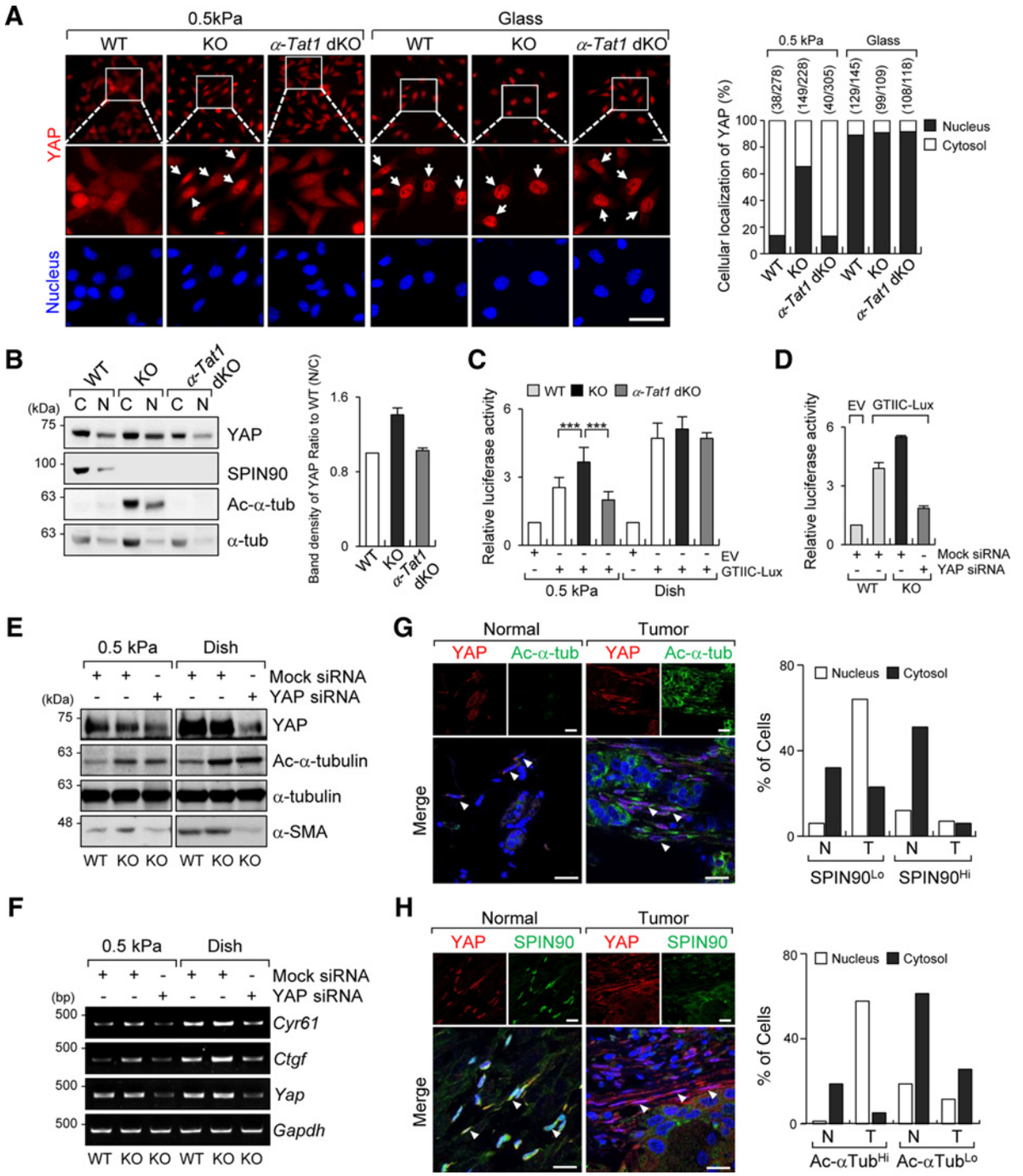

Figure 5.

Spin90 deficiency–mediated microtubule acetylation promotes YAP activity in low stiffness matrices. **A,** Images show YAP cellular localization (red) and nucleus (blue) in WT, *Spin90*-KO, and *α-Tat1*-dKO MEFs. White arrows, nuclear accumulation of YAP. Graphs show YAP cellular localization. **B,** Cytosolic/nuclear fractionation of WT, *Spin90*-KO, *α-Tat1*-dKO MEFs on 0.5 kPa PAGs. C, cytosolic fraction; N, nuclear fraction. **C,** Luciferase reporter assay (8xGTIIC-Lux) in WT, *Spin90*-KO, *α-Tat1*-dKO MEFs to measure YAP transcriptional activity. ***, $P < 0.001$. **D,** WT and *Spin90*-KO MEFs were transfected with siRNA (mock and YAP) and either pGL3-empty vector (EV) or 8xGTIIC-Lux. **E,** Western blots, levels of YAP, Ac-α-tub, and α-SMA in WT and *Spin90 KO* MEFs transfected with either mock or YAP siRNA. **F,** Gene expression levels (*Cyr61, Ctgf,* and *Yap*) in indicated siRNA-transfected WT and *Spin90-KO* MEFs were compared with RT-PCR. **G** and **H,** Breast cancer tissues ($n = 30$) were subjected to double staining with anti-YAP and anti–Ac-α-tub (**G**), and anti-YAP and anti-SPIN90 (**H**) antibodies and followed by Alexa-555 and Alexa-488 dyes, respectively. Fluorescence intensity were measured and analyzed by MetaMorph software.

Published OnlineFirst June 26, 2017; DOI: 10.1158/0008-5472.CAN-17-0657

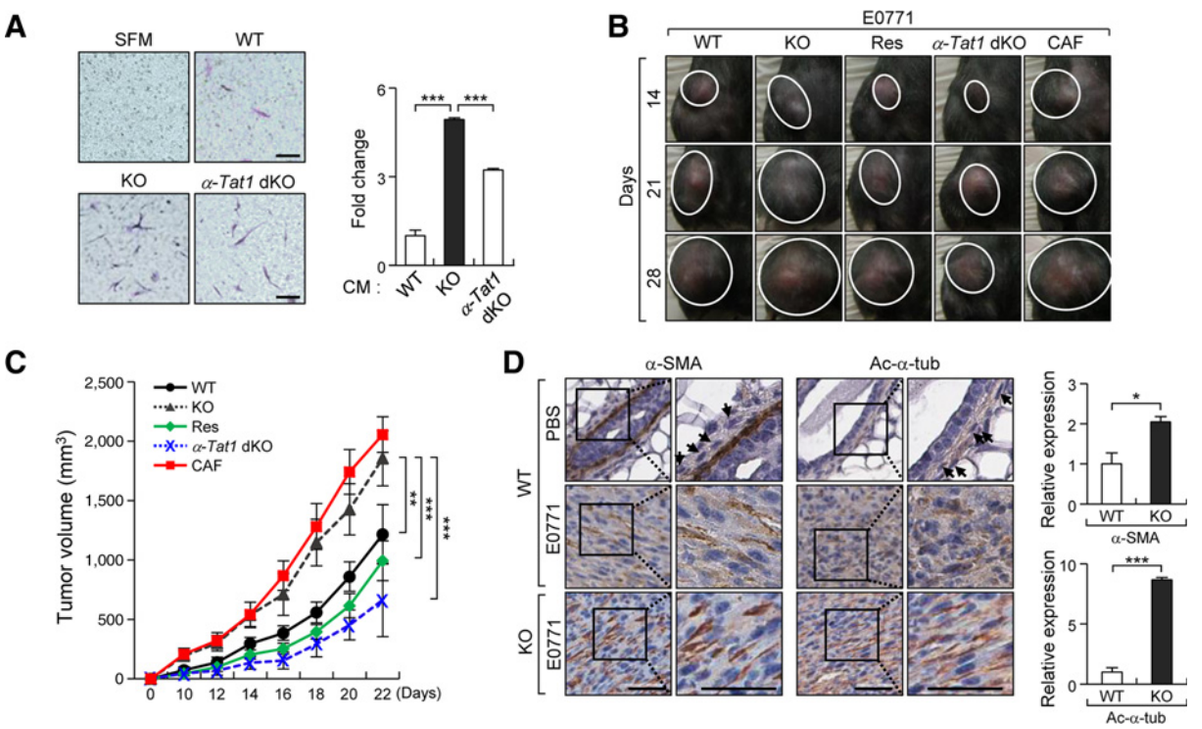

Figure 6.

Increased α-tubulin acetylation in *Spin90*-KO MEFs induces cancer progression. **A,** Invasion of MDA-MB-231 cells was examined using a modified Boyden chamber assay with CM from WT, *Spin90*-KO, and *α-Tat1*-dKO MEFs. Scale bar, 100 μm. **B** and **C,** Orthotopic injection of E0771 cells with MEFs (WT, *Spin90*-KO, rescued, and *α-Tat1*-dKO) and CAFs as a positive control in a murine breast cancer model. Representative images (**B**) and progression of developing tumor volume (**C**). **D,** Immunohistochemistry analysis with anti–α-SMA and anti–acetyl-α-tubulin antibodies in paraffin sections of orthotopic breast tumors. Scale bar, 60 μm. *, $P \leq 0.05$; **, $P \leq 0.01$; ***, $P \leq 0.001$.

FN-coated PAGs with a Young's modulus of ∼0.5 kPa representing the approximate stiffness of normal breast stroma (6). 20 kPa representing the approximate stiffness of malignant breast tumor (8) and on glass coverslips (∼10^6 kPa; ref. 21). *Spin90*$^{-/-}$ MEFs cultured on 0.5 kPa PAG displayed slender morphology with increased protrusions at the periphery while WT MEFs were rounded in shape (Fig. 3A and B; Supplementary Fig. S3A). No significant morphologic differences were observed in cells cultured on glass coverslips. Notably, *α-Sma* and other myofibroblast markers, including *Ctgf* and *Cyr61*, were highly expressed in *Spin90*$^{-/-}$ MEFs under 0.5 kPa PAG (Fig. 3C–E; Supplementary Fig. S3B and S3C).

It has been reported that CAFs can be classified into two subtypes, myofibroblastic CAFs [α-SMA^{high}/IL6^{low}] and inflammatory CAFs (α-SMA^{low}/IL6^{high}), which serve distinct roles in cancer progression (24). To determine the CAF linage of *Spin90*$^{-/-}$ MEFs, we examined expression of the markers of inflammatory CAFs such as *Il6* and *Il11*. *Spin90*$^{-/-}$ MEFs expressed low levels of *Il6*, but did not express detectable levels of *Il11*, indicating that *Spin90*$^{-/-}$ MEFs exhibit a myofibroblastic CAF phenotype (α-SMA^{high}/IL6^{low}) rather than an inflammatory CAF phenotype (Supplementary Fig. S3D).

A comparison of the contractile activities of WT and *Spin90*$^{-/-}$ MEFs by analysis of FMC and SMC (22) revealed higher cellular contractility of *Spin90*$^{-/-}$ MEFs compared with WT cells using BSA instead of FBS (Fig. 3F). However, the contractility of both cell groups in procontractile conditions (e.g., in the presence of FBS) was similar (Fig. 3F), indicating that MEFs develop intrinsic cellular contractility due to SPIN90 loss, which may influence myofibroblast differentiation under soft matrix conditions.

Next, we examined the cancer cell invasive and migratory activity using the Boyden chamber assay and a 3D organotypic culture system. CM were collected by *in vitro* culture of MEF isolated from WT and *Spin90*$^{-/-}$ mice. CM obtained from *Spin90*$^{-/-}$ MEFs were sufficient to induce invasion of MDA-MB-231 cancer cells (Supplementary Fig. S3E). In contrast, CM from WT and SPIN90-rescued MEFs (Res) were not effective in inducing invasion. In accordance with these data, 3D organotypic culture that closely mimics the physiologic tumor microenvironment (23), cancer cell invasion was increased in collagen gels embedded with *Spin90*$^{-/-}$ MEFs (Fig. 3G).

Microtubule acetylation is critical for myofibroblast differentiation

We examined the effects of SPIN90 deficiency on α-tubulin posttranslational modifications, such as tubulin acetylation and detyrosination, representing well-known mechanisms for increasing microtubule stability. Acetylated, but not detyrosinated α-tubulin was significantly increased in *Spin90*$^{-/-}$ MEFs cultured on 0.5 kPa PAG (Fig. 4A), thereby leading to acquisition of resistance to nocodazole treatment (Supplementary Fig. S4A). Rescue of SPIN90 expression in *Spin90*$^{-/-}$ MEF led to a dramatic decrease in the acetylated α-tubulin level (Fig. 4B), clearly indicating that SPIN90 deficiency affects microtubule stability.

Published OnlineFirst June 26, 2017; DOI: 10.1158/0008-5472.CAN-17-0657

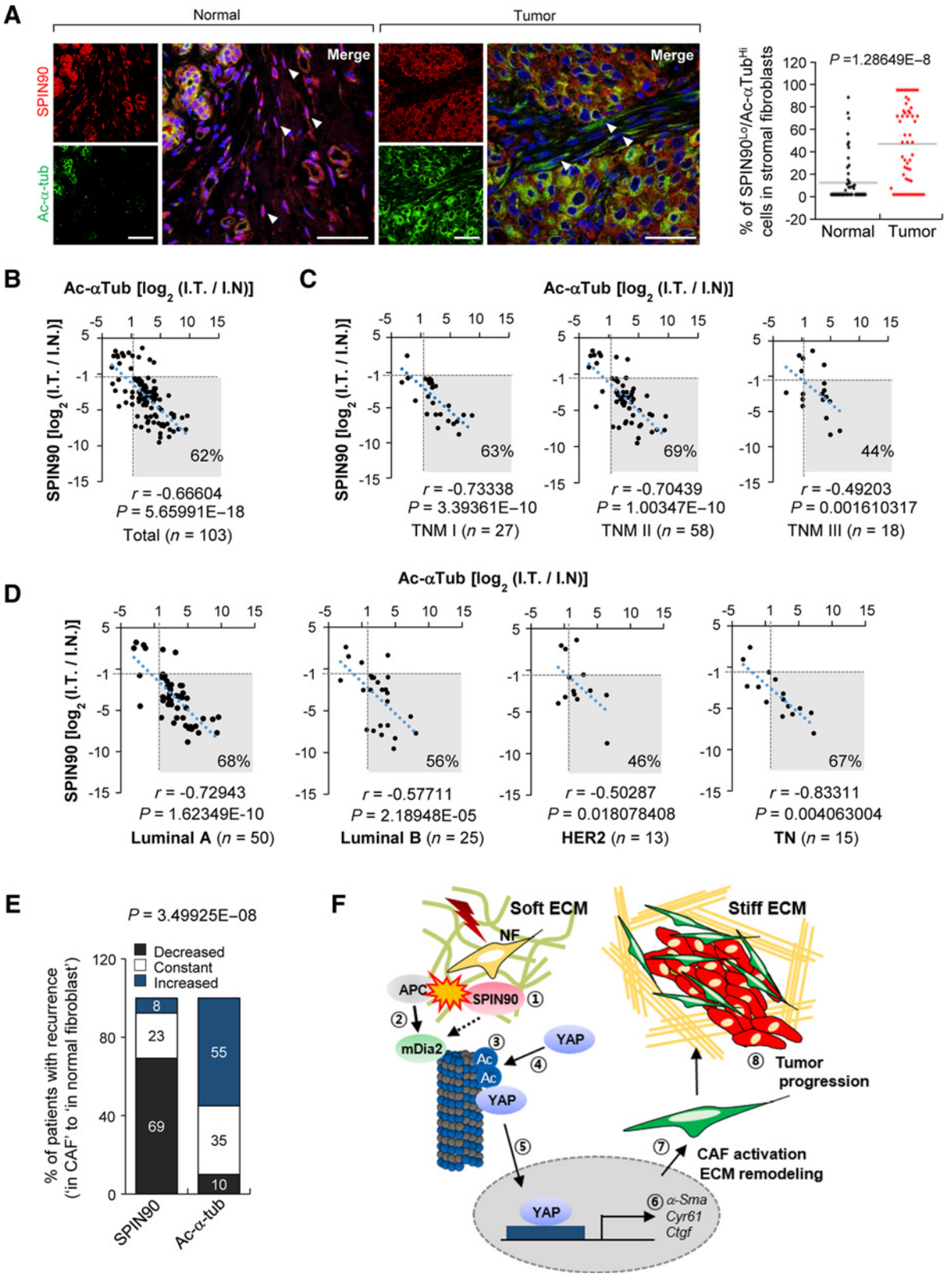

Published OnlineFirst June 26, 2017; DOI: 10.1158/0008-5472.CAN-17-0657

We generated *Spin90* and *α-tubulin acetyltransferase 1 (α-Tat1)*-double KO MEFs (*α-Tat1*-dKO) using the CRISPR/Cas9 system (Supplementary Fig. S4B). *Spin90*-KO–mediated cell spreading on soft substrate was completely abrogated in both SPIN90-rescued and *α-Tat1*-dKO cells (Fig. 4C). Nuclear deformation, which reflects cell elongation (25), was observed infrequently in both SPIN90-rescued and *α-Tat1*-dKO MEFs (Fig. 4C). In addition, expression of α-SMA and myofibroblast marker genes observed in *Spin90*$^{-/-}$ MEFs was completely inhibited in *α-Tat1*-dKO cells (Fig. 4D), consistent with the significant suppression of collagen gel contraction in *α-Tat1*-dKO MEFs (Fig. 4E).

Earlier studies reported that acetylated tubulins accumulate in stable microtubules (26) and that members of the mDia family regulate microtubule stability in association with various microtubule-binding proteins (27, 28). Accordingly, we investigated the molecular mechanisms underlying the association of mDia with microtubule acetylation under conditions of SPIN90 deficiency. Treatment with a pharmacologic inhibitor of the formin family (smiFH2) inhibited microtubule acetylation under SPIN90 depletion (Supplementary Fig. S4C) and resulted in reduced production of nocodazole-resistant microtubules (Supplementary Fig. S4A). Spreading of *Spin90*$^{-/-}$ MEFs on soft substrates was also significantly impaired by smiFH2, which was rescued by overexpression of the α-tubulin acetyl-mimic (K40Q) mutant (Supplementary Fig. S4D; ref. 29). The data indicate that mDia is required for both SPIN90-associated microtubule acetylation and cell spreading in soft substrates. Experiments performed on *Spin90*$^{-/-}$ MEFs transfected with siRNAs targeting mDia1 and mDia2 confirmed that mDia2 is specifically involved in microtubule acetylation (Supplementary Fig. S4E). Genetic disruption of *mDia2* using the CRISPR/Cas9 system (Supplementary Fig. S4B) in *Spin90*$^{-/-}$ MEFs (*mDia2*-dKO) prevented SPIN90 deficiency–mediated cell spreading and nuclear deformation (Fig. 4F; Supplementary Fig. S4F). Additionally, knockout or knockdown of *mDia2* in *Spin90*$^{-/-}$ MEFs reduced expression of α-SMA (Fig. 4G; Supplementary Fig. S4G) and collagen matrix contraction (Fig. 4H), indicating that mDia2 plays an essential role in microtubule acetylation with SPIN90 depletion.

Interactions of mDia with APC and EB1 via its FH1 and FH2 domains are involved in microtubule stabilization and modification (28). SPIN90 also directly binds the FH1 and FH2 domain of mDia, which is known to regulate actin dynamics (30). In view of these findings, we speculated that SPIN90 competes with APC for binding to mDia. Indeed, interactions of mDia2 with APC in *Spin90*$^{-/-}$ MEFs were enhanced (Fig. 4I), whereas overexpression of SPIN90 in *Spin90*$^{-/-}$ MEFs suppressed this binding in a manner dependent on SPIN90 levels (Fig. 4J). Next, we examined whether APC-bound mDia2 preferably binds to microtubule in the absence of SPIN90. The recruitment of mDia2 to microtubules in *Spin90*$^{-/-}$ MEFs on soft matrices was assessed by *in vivo* microtubule sedimentation assay. When the F-actin level was relatively low, mDia2 was found in the pellet fraction with microtubules. Cosedimentation of mDia2 with microtubules was enhanced in *Spin90*$^{-/-}$ cells, which was reversed in the *α-Tat1*-dKO MEFs (Fig. 4K). In addition, acetylated tubulin was observed in the cosedimented fraction of mDia2 in *Spin90*$^{-/-}$ cells. Our results collectively indicate that SPIN90 deficiency facilitates the formation of APC/mDia2 complexes, which lead to enhance their accessibility toward microtubules (Supplementary Fig. S4H).

SPIN90 deficiency–mediated microtubule acetylation promotes YAP activity in low stiff matrices

Next, we determined the underlying mechanism by which SPIN90 deficiency–mediated microtubule acetylation promotes myofibroblast differentiation. In this study, nuclear translocation of YAP markedly increased in *Spin90*$^{-/-}$ MEFs even on soft matrices but it was reversed in *α-Tat1*-dKO cells. However, YAP mostly localized in the nucleus in all types of cells on glass coverslips independent of microtubule acetylation (Fig. 5A; Supplementary Fig. S5A). This was confirmed by cellular fractionation assay showing increased YAP in nuclear fraction of *Spin90*$^{-/-}$ cells (Fig. 5B). Overexpression of α-TAT1 and acetyl-mimic α-tubulin (K40Q) in WT MEF facilitated nuclear localization of YAP in 0.5 kPa soft PAG matrices (Supplementary Fig. S5B–S5D). For a direct readout of YAP activity, we used a YAP-responsive luciferase reporter (8XGTIIC-lux). YAP activity increased in *Spin90*$^{-/-}$ MEFs on soft matrices but it was reversed by *α-Tat1* depletion (Fig. 5C). YAP silencing with siRNA reduced YAP-responsive reporter activity (Fig. 5D) and inhibited α-SMA expression (Fig. 5E) as well as the expression of myofibroblast marker genes such as *Ctgf* and *Cyr61* (Fig. 5F) on low stiffness matrices. Next, we examined YAP localization in CAFs within human breast cancer stroma. Cytoplasmic localization of YAP was mostly observed in fibroblasts with low level of α-tubulin acetylation in normal breast stroma, whereas YAP mainly localized in the nucleus of cells with highly acetylated tubulin in tumor stroma (approximately 60% cells among overall selected cells, $n = 30$; Fig. 5G). Consistently, cellular localization of YAP correlated with SPIN90 expression in fibroblasts. Nuclear translocation of YAP was mainly observed in long spindle shaped SPIN90^{Lo} CAFs within tumor stroma ($n = 30$; Fig. 5H). These data collectively support that acetylated

Figure 7.

Regulation of SPIN90 and α-tubulin acetylation in human breast cancer stroma. **A,** Breast cancer tissues ($n = 30$) were subjected to immunohistochemistry with anti-SPIN90 and anti–Ac-α-tub antibodies and followed by Alexa-555 and Alexa-488 dyes, respectively. Fluorescence intensities were measured and analyzed by MetaMorph software. **B–D,** An analysis of IHC images of human breast cancer tissues in tissue microarrays revealed a negative correlation between SPIN90 downregulation and α-tubulin acetylation. Scatter plots of data for all patients ($n = 103$; **B**), based on TNM stage (**C**) or molecular subtype (**D**), are displayed with Pearson correlation coefficient (r) and statistical significance of r (P value). An absolute value of $\log_2$ (I.T./I.N.) greater than 1 indicates at least a two-fold increase in α-tubulin acetylation or a two-fold decrease in SPIN90 expression compared with normal stroma. The gray-shaded box shows the proportion of patients satisfying the above criteria. **E,** Percent changes in SPIN90 expression and acetylated α-tubulin in tumor stroma compared with paired normal tissue in cancer tissue samples were analyzed in patients with recurrence ($n = 26$). Tissues were obtained from surgery performed at the time of the initial diagnosis. **F,** Proposed model for SPIN90-mediated CAF differentiation in cancer stroma. ①–②, Downregulation of SPIN90 in early stage of cancer stroma, which facilitates the formation of APC-mDia2 complex. ③, mDia2–APC complex binds to microtubules and increased microtubule acetylation, leading to stabilization. ④–⑥, Acetylated MT facilitates YAP nuclear translocation of YAP, resulting in expression of myofibroblastic marker genes. ⑦–⑧, Activated CAFs remodel stromal ECM, which favors tumor progression in an early stage of cancer.

Published OnlineFirst June 26, 2017; DOI: 10.1158/0008-5472.CAN-17-0657

microtubules induced by SPIN90 depletion facilitates nuclear translocation of YAP and its target gene expression on low stiffness matrices.

α-tubulin acetylation in *Spin90*-deficient MEFs promotes cancer progression

To further clarify the relationship between microtubule acetylation and CAF formation, experiments were performed to determine whether *α-Tat1*-dKO cells are devoid of CAF activity. CM obtained from *α-Tat1*-dKO MEFs was not effective on invasion of MDA-MB-231 cells (Fig. 6A). In an orthotopic breast cancer model, coinjection of E0771 cells with *Spin90*$^{-/-}$ MEFs induced the formation of large tumors with similar sizes to those observed upon coinjection with CAFs obtained from orthotopic breast tumors, whereas coinjection with SPIN90-rescued or *α-Tat1*-dKO MEFs resulted in the formation of small tumors (Fig. 6B and C; Supplementary Fig. S6A). Distinct increases in tumor volume in the *Spin90*$^{-/-}$ MEF and CAF groups were observed during initial tumor growth, determined from days 10 to 18 (Fig. 6C). These results indicate that MEFs obtained from *Spin90*$^{-/-}$ mice display more of a CAF-like phenotype. Consistent with this observation, increased α-SMA expression in orthotopic tumors from *Spin90*$^{-/-}$ mice was observed, compared with those of WT controls (Fig. 6D). This finding was also true for acetylated α-tubulin, as determined based on immunohistochemistry analysis (Fig. 6D). Enhanced α-SMA expression and acetylated α-tubulin were additionally prevalent in sections of lung metastases from *Spin90*$^{-/-}$ mice (Supplementary Fig. S6B).

Regulation of SPIN90 and α-tubulin acetylation in CAFs within human cancer stroma

Increased α-tubulin acetylation was observed in SPIN90^{Lo} CAFs (low or no expression of SPIN90) of human breast cancer stroma (Fig. 7A). In normal stromal fibroblasts, SPIN90 was highly expressed while acetylation of α-tubulin was significantly low. As shown in Fig. 7A, SPIN90^{Lo} and Ac-α-tub^{Hi} cells were abundant in CAFs within tumor stroma ($n = 30$). To further determine whether SPIN90 expression and tubulin acetylation are associated with progression of human breast cancer, we compared SPIN90 expression and acetylation of α-tubulin in normal stromal fibroblasts and CAFs obtained from patients diagnosed with breast cancer in 2008 or 2009 ($n = 103$). Among patients, 62% showed both a decrease in SPIN90 and an increase in acetylated α-tubulin in tumor stroma greater than 2 times that in normal stroma (Fig. 7B). Pearson correlation tests revealed a negative correlation between SPIN90 expression and acetylation of α-tubulin ($r = -0.66604$, $P = 5.7 \times 10^{-18}$; Fig. 7B). Samples were further analyzed based on tumor node metastasis (TNM) stage. Overall, 63% stage I, 69% stage II, and 44% stage III samples showed decreased SPIN90 expression and increased acetylated α-tubulin in cancer stroma CAFs (Fig. 7C). Downregulation of SPIN90 and increased acetylated α-tubulin were prominent in TNM stages I and II, but not stage III. An analysis of samples by subgrouping into four molecular subtypes of breast cancer related to prognosis and recurrence revealed a significant decrease in SPIN90 and increase in acetylated α-tubulin in CAFs from luminal A ($r = -0.72943$, $P = 1.62349E\text{-}10$) and triple-negative ($= -0.83311$, $P = 0.00406$) subtypes (Fig. 7D). Stroma participates in therapeutic resistance, which contributes to breast cancer progression and poor prognosis (31, 32). Of the 103 patients examined, 26 had recurrence within 5 years. In patients with cancer recurrence, decreased expression of SPIN90 (69.2%, 18/26) and increased acetylation of α-tubulin (55%, 11/20) in CAFs compared with paired normal stromal fibroblasts were prominent (Fig. 7E). Taken together, the data suggest that the SPIN90/acetylated α-tubulin axis in CAFs is significantly involved in breast cancer progression (Fig. 7F)

Discussion

Myofibroblasts contain actin bundles with contractile units, including nonmuscle myosin and α-SMA, and their contractility promotes mechanical remodeling of the surrounding ECM during cancer development. Fibroblasts in normal stroma (mechanically soft condition) are devoid of focal adhesion and stress fibers (via actin polymerization; ref. 33) and instead, microtubule-mediated cell spreading and signaling are dominant in the 3D compliant and soft substrate environments, such as normal stroma (10, 11). In particular, microtubule acetylation in soft substrate appears essential for gene expression as well as cell spreading for myofibroblast differentiation (34, 35). In support of this idea, disruption of microtubule acetylation via *α-Tat1* ablation in soft substrate conditions completely inhibited cell spreading, α-SMA expression and cellular contractility assessed based on 3D collagen gel contraction. We reason that microtubule acetylation possibly offers a stable microtubule network for gene expression by regulating cellular trafficking of transcription factors essential for myofibroblast differentiation, such as YAP, in soft matrices.

A mechanosensor YAP localizes in cytoplasm on low stiffness matrices (17) and translocates into the nucleus depending on matrix stiffness. In this study, we demonstrated that YAP localized in the nucleus of *Spin90*-deficient cells even on soft matrices. Nuclear translocation of YAP enhanced the expression of myofibroblast marker genes, such as *α-Sma*, *Cyr61*, and *Ctgf*, which are responsible for the acquisition of myofibroblast phenotypes. On soft matrices, YAP, thus, is likely to sense cellular contractility induced by acetylated microtubules on the matrices with low stiffness, but not by actin cytoskeletons. This could explain how stromal fibroblasts acquire the properties of CAF in stroma with relatively low stiffness of early stage breast cancer.

In our experiments, *Spin90*$^{-/-}$ MEFs contained stable and acetylated microtubules resistant to nocodazole. Moreover, *Spin90*$^{-/-}$ MEFs exerted a strong contractile force in collagen matrix contraction, which was abolished upon inhibition of tubulin acetylation. Suppression of SPIN90 expression with siRNA strongly enhanced stress fiber formation, indicative of RhoA activation (36). These results are inconsistent with previous reports that disruption of microtubule networks induces RhoA activity, leading to enhanced focal adhesion formation and contractility in cells, and a decrease in cellular contractility induced by blebbistatin in human dermal fibroblasts results in increased microtubule acetylation (29). These discrepancies in results from different studies imply that cell contractility and/or spreading are not mediated by a common cellular mechanism in soft matrix and stiff matrix conditions.

Published OnlineFirst June 26, 2017; DOI: 10.1158/0008-5472.CAN-17-0657

Based on the current findings, we reason that depletion of SPIN90 in soft matrix conditions (normal stroma) facilitates interactions of mDia2 with APC. The mDia/APC complex enhances microtubule stability and modification, consequently driving YAP activation for myofibroblast differentiation. Activated myofibroblasts have high synthetic capacity for ECM proteins, deposition of collagen as well as tissue remodeling. Environmental stiffness is gradually increased, stress fibers and focal adhesions develop, and subsequently, surrounding normal fibroblasts are activated (37).

Reciprocal interactions between stromal fibroblasts and tumor cells occur at the initial stages of cancer progression. With respect to CAF functions, in the traditional view, the tumor stroma is considered to be protumorigenic (38, 39); however, the potential of tumor stroma to exert antitumorigenic properties has been suggested in the context of pancreatic cancer. For instance, α-SMA^{+}-CAF depletion in a mouse pancreatic cancer model was shown to promote cancer progression and decrease survival by altering tumor immunity, suggesting antitumorigenic functions of CAFs (40, 41). These apparent differences in the properties of stromal CAFs may reflect the effects of the distinct microenvironments of different cancers. In light of such context dependence, pro- or antitumorigenic functions of CAFs should be carefully considered in cancer therapy strategies targeting CAFs. In our study, *Spin90*$^{-/-}$ MEFs differentiated into myofibroblastic CAFs with α-SMA^{high}/(IL)-6^{low} expression and exhibited pro-tumorigenic properties in breast cancer. Enhanced tumor formation in *Spin90*$^{-/-}$ mice was prominent at an early stage after tumor injection (Fig. 2). The effects of SPIN90 deficiency on fibroblasts were confirmed by coinjection of cancer cells and *Spin90*$^{-/-}$ MEFs into WT mice, which promoted tumor formation, similar to that observed with coinjection of CAFs. These data support the theory that coinjected MEFs in mammary fat pads are primed by the cancer cells and undergo transition to CAF. Coinjected *Spin90*$^{-/-}$ MEF have greater CAF activity, and may, therefore, alter the ECM composition and stiffness to promote cancer progression. In addition, inhibition of microtubule acetylation in *α-Tat1*-dKO MEFs significantly blocked tumor formation in an E0771 breast cancer model.

Therapeutic approaches for targeting both cancer cells and CAFs have continued to expand, and although the current study did not clarify the mechanism underlying SPIN90 downregulation in CAFs, the control of CAF activation through regulation of SPIN90 expression may ultimately provide a novel option for effective treatment of early-stage breast cancer. Signals induced by infection or chronic inflammation activate normal fibroblasts as well as cancer and/or inflammatory cells within the tumor microenvironment at the early stage of cancer (4). These primed cells reciprocally or mutually interact with each other through paracrine signaling. For example, TGFβ1 secreted by many cell types, including macrophages and cancer cells, is a major inducer of stromal fibroblast activation and resulting CAF differentiation (7). However, we found that TGFβ1 did not suppress SPIN90 expression in WT MEFs (data not shown). Instead, we identified circular miRNAs as potential suppressors of SPIN90 expression in a mouse breast cancer model. Thus, we speculate that other growth factors, cytokines, or miRNAs secreted by adjacent inflammatory cells and/or cancer cells in the tumor microenvironment may regulate SPIN90 expression in stromal fibroblasts at the early stage of cancer; however, this still remains to be demonstrated experimentally.

Tumor stroma is known to contribute to drug resistance and poor prognosis. Stromal activation is a major factor associated with cancer recurrence within 5 years, despite administration of the appropriate treatments (38). Collagen type I, secreted by CAFs, promotes the formation of a stiff tumor microenvironment, which, in turn, inhibits chemotherapeutic drug uptake and regulates tumor sensitivity to chemotherapy (40). Treatment with anticancer drugs such as tamoxifen and trastuzumab has greatly improved overall survival but ~33% of patients still experience recurrence and metastasis (42). In this study, downregulation of SPIN90 and increased α-tubulin acetylation in CAFs were observed in more than 55% of patients with cancer recurrence, an observation with implications for therapeutics to prevent recurrence. In conclusion, our current findings offer new insights into the control of CAF activation through regulation of SPIN90 expression and microtubule acetylation in breast cancer stroma.

Disclosure of Potential Conflicts of Interest

No potential conflicts of interest were disclosed.

Authors' Contributions

Conception and design: E. You, Y.H. Huh, S. Rhee, W.K. Song
Development of methodology: E. You, Y.H. Huh, J.-H. Ryu, S. Rhee, W.K. Song
Acquisition of data (provided animals, acquired and managed patients, provided facilities, etc.): E. You, Y.H. Huh, O.-J. Lee, J.-H. Ryu, M.H. Park, G.-E. Kim, J.S. Lee, K.H. Lee, W.K. Song
Analysis and interpretation of data (e.g., statistical analysis, biostatistics, computational analysis): E. You, Y.H. Huh, A. Kwon, J.-H. Ryu, K.H. Lee, Y.-S. Lee, J.-W. Kim, S. Rhee, W.K. Song
Writing, review, and/or revision of the manuscript: E. You, Y.H. Huh, S. Rhee, W.K. Song
Administrative, technical, or material support (i.e., reporting or organizing data, constructing databases): A. Kwon, I.H. Chae, S. Rhee
Study supervision: Y.H. Huh, S. Rhee, W.K. Song

Acknowledgments

We thank Dr. Henry N. Higgs (Dartmouth Medical School) for the anti-mDia2 antibody, Dr. Shuh Narumiya (Kyoto University) for the GFP-mDia2 construct, Dr. Phillippe Chavrier (Institut Curie, Research Center) for the GFP-αTAT1 construct, and Dr. Kenneth M. Yamada (NIH) for GFP-α-tubulin (K40A) and GFP-α-tubulin (K40Q) constructs.

Grant Support

This research was supported by the National Research Foundation of Korea (S. Rhee, NRF-2014R1A2A1A11050606 and NRF-2016R1A4A1008035), Bio Imaging and Cell Logistics Research Center (W.K. Song, NRF-2016R1A5A1007318), Brain Research Program (W.K. Song, NRF-2013M3C7A1073001), Mid-Career Research Program (NRF-2014R1A2A2A01004969), and Basic Science Research Program (Y.H. Huh, NRF-2016R1C1B1013237) through the National Research Foundation of Korea funded by the Ministry of Science, ICT & Future Planning, and also supported by Chung-Ang University Excellent Student Scholarship in 2013 (E. You).

The costs of publication of this article were defrayed in part by the payment of page charges. This article must therefore be hereby marked *advertisement* in accordance with 18 U.S.C. Section 1734 solely to indicate this fact.

Received March 3, 2017; revised April 26, 2017; accepted June 20, 2017; published OnlineFirst June 26, 2017.

Published OnlineFirst June 26, 2017; DOI: 10.1158/0008-5472.CAN-17-0657

References

1. Castello-Cros R, Cukierman E. Stromagenesis during tumorigenesis: characterization of tumor-associated fibroblasts and stroma-derived 3D matrices. Methods Mol Biol 2009;522:275–305.
2. Levental KR, Yu H, Kass L, Lakins JN, Egeblad M, Erler JT, et al. Matrix crosslinking forces tumor progression by enhancing integrin signaling. Cell 2009;139:891–90.
3. Paszek MJ, Zahir N, Johnson KR, Lakins JN, Rozenberg GI, Gefen A, et al. Tensional homeostasis and the malignant phenotype. Cancer Cell 2005;8:241–54.
4. Beacham DA, Cukierman E. Stromagenesis: the changing face of fibroblastic microenvironments during tumor progression. Semin Cancer Biol 2005;15:329–41.
5. Kalluri R, Zeisberg M. Fibroblasts in cancer. Nat Rev Cancer 2006; 6:392–401.
6. Alcoser TA, Bordeleau F, Carey SP, Lampi MC, Kowal DR, Somasegar S, et al. Probing the biophysical properties of primary breast tumor-derived fibroblasts. Cell Mol Bioeng 2015;8:76–85.
7. Thannickal VJ, Lee DY, White ES, Cui Z, Larios JM, Chacon R, et al. Myofibroblast differentiation by transforming growth factor-beta1 is dependent on cell adhesion and integrin signaling via focal adhesion kinase. J Biol Chem 2003;278:12384–9.
8. Chandler EM, Seo BR, Califano JP, Andresen Eguiluz RC, Lee JS, Yoon CJ, et al. Implanted adipose progenitor cells as physicochemical regulators of breast cancer. Proc Natl Acad Sci U S A 2012;109:9786–91.
9. Tschumperlin DJ.Fibroblasts and the ground they walk on. Physiology (Bethesda) 2013;28:380–90.
10. Rhee S, Jiang H, Ho CH, Grinnell F. Microtubule function in fibroblast spreading is modulated according to the tension state of cell–matrix interactions. Proc Natl Acad Sci U S A 2007;104:5425–30.
11. Wang N, Naruse K, Stamenovic D, Fredberg JJ, Mijailovich SM, Tolic-Norrelykke IM, et al. Mechanical behavior in living cells consistent with the tensegrity model. Proc Natl Acad Sci U S A 2001;98:7765–70.
12. Kraning-Rush CM, Carey SP, Califano JP, Smith BN, Reinhart-King CA. The role of the cytoskeleton in cellular force generation in 2D and 3D environments. Phys Biol 2011;8:015009.
13. Even-Ram S, Doyle AD, Conti MA, Matsumoto K, Adelstein RS, Yamada KM. Myosin IIA regulates cell motility and actomyosin-microtubule crosstalk. Nat Cell Biol 2007;9:299–309.
14. Boggs AE, Vitolo MI, Whipple RA, Charpentier MS, Goloubeva OG, Ioffe OB, et al. alpha-Tubulin acetylation elevated in metastatic and basal-like breast cancer cells promotes microtentacle formation, adhesion, and invasive migration. Cancer Res 2015;75:203–15.
15. Zhang Z, Yamashita H, Toyama T, Sugiura H, Omoto Y, Ando Y, et al. HDAC6 expression is correlated with better survival in breast cancer. Clin Cancer Res 2004;10:6962–8.
16. Schroeder MC, Halder G. Regulation of the Hippo pathway by cell architecture and mechanical signals. Semin Cell Dev Biol 2012;23: 803–11.
17. Dupont S, Morsut L, Aragona M, Enzo E, Giulitti S, Cordenonsi M, et al. Role of YAP/TAZ in mechanotransduction. Nature 2011;474:179–83.
18. Halder G, Dupont S, Piccolo S. Transduction of mechanical and cytoskeletal cues by YAP and TAZ. Nat Rev Mol Cell Biol 2012;13:591–600.
19. Maller O, DuFort CC, Weaver VM. YAP forces fibroblasts to feel the tension. Nat Cell Biol 2013;15:570–2.
20. Calvo F, Ege N, Grande-Garcia A, Hooper S, Jenkins RP, Chaudhry SI, et al. Mechanotransduction and YAP-dependent matrix remodelling is required for the generation and maintenance of cancer-associated fibroblasts. Nat Cell Biol 2013;15:637–46.
21. Tse JR, Engler AJ. Preparation of hydrogel substrates with tunable mechanical properties. Curr Protoc Cell Biol 2010;Chapter 10:Unit 10 6.
22. Rhee S, Grinnell F. P21-activated kinase 1: convergence point in PDGF- and LPA-stimulated collagen matrix contraction by human fibroblasts. J Cell Biol 2006;172:423–32.
23. Nurmenniemi S, Sinikumpu T, Alahuhta I, Salo S, Sutinen M, Santala M, et al. A novel organotypic model mimics the tumor microenvironment. Am J Pathol 2009;175:1281–91.
24. Ohlund D, Handly-Santana A, Biffi G, Elyada E, Almeida AS, Ponz-Sarvise M, et al. Distinct populations of inflammatory fibroblasts and myofibroblasts in pancreatic cancer. J Exp Med 2017;214:579–96.
25. Versaevel M, Grevesse T, Gabriele S. Spatial coordination between cell and nuclear shape within micropatterned endothelial cells. Nat Commun 2012;3:671.
26. Palazzo AF, Cook TA, Alberts AS, Gundersen GG. mDia mediates Rho-regulated formation and orientation of stable microtubules. Nat Cell Biol 2001;3:723–9.
27. Thurston SF, Kulacz WA, Shaikh S, Lee JM, Copeland JW. The ability to induce microtubule acetylation is a general feature of formin proteins. PLoS One 2012;7:e48041.
28. Wen Y, Eng CH, Schmoranzer J, Cabrera-Poch N, Morris EJ, Chen M, et al. EB1 and APC bind to mDia to stabilize microtubules downstream of Rho and promote cell migration. Nat Cell Biol 2004;6:820–30.
29. Joo EE, Yamada KM. MYPT1 regulates contractility and microtubule acetylation to modulate integrin adhesions and matrix assembly. Nat Commun 2014;5:3510.
30. Eisenmann KM, Harris ES, Kitchen SM, Holman HA, Higgs HN, Alberts AS. Dia-interacting protein modulates formin-mediated actin assembly at the cell cortex. Curr Biol 2007;17:579–91.
31. Martinez-Outschoorn UE, Pavlides S, Howell A, Pestell RG, Tanowitz HB, Sotgia F, et al. Stromal-epithelial metabolic coupling in cancer: integrating autophagy and metabolism in the tumor microenvironment. Int J Biochem Cell Biol 2011;43:1045–51.
32. Sun Y, Campisi J, Higano C, Beer TM, Porter P, Coleman I, et al. Treatment-induced damage to the tumor microenvironment promotes prostate cancer therapy resistance through WNT16B. Nat Med 2012;18:1359–68.
33. Prager-Khoutorsky M, Lichtenstein A, Krishnan R, Rajendran K, Mayo A, Kam Z, et al. Fibroblast polarization is a matrix-rigidity-dependent process controlled by focal adhesion mechanosensing. Nat Cell Biol 2011;13: 1457–65.
34. Wloga D, Gaertig J. Post-translational modifications of microtubules. J Cell Sci 2010;123:3447–55.
35. Perdiz D, Mackeh R, Pous C, Baillet A. The ins and outs of tubulin acetylation: more than just a post-translational modification? Cell Signal 2011;23:763–71.
36. Teodorof C, Bae JI, Kim SM, Oh HJ, Kang YS, Choi J, et al. SPIN90-IRSp53 complex participates in Rac-induced membrane ruffling. Exp Cell Res 2009;315:2410–9.
37. Huang X, Yang N, Fiore VF, Barker TH, Sun Y, Morris SW, et al. Matrix stiffness-induced myofibroblast differentiation is mediated by intrinsic mechanotransduction. Am J Respir Cell Mol Biol 2012;47:340–8.
38. Mao Y, Keller ET, Garfield DH, Shen K, Wang J. Stromal cells in tumor microenvironment and breast cancer. Cancer Metastasis Rev 2013; 32:303–15.
39. Loeffler M, Kruger JA, Niethammer AG, Reisfeld RA. Targeting tumor-associated fibroblasts improves cancer chemotherapy by increasing intratumoral drug uptake. J Clin Invest 2006;116:1955–62.
40. Ozdemir BC, Pentcheva-Hoang T, Carstens JL, Zheng X, Wu CC, Simpson TR, et al. Depletion of carcinoma-associated fibroblasts and fibrosis induces immunosuppression and accelerates pancreas cancer with reduced survival. Cancer Cell 2014;25:719–34.
41. Rhim AD, Oberstein PE, Thomas DH, Mirek ET, Palermo CF, Sastra SA, et al. Stromal elements act to restrain, rather than support, pancreatic ductal adenocarcinoma. Cancer Cell 2014;25:735–47.
42. Early Breast Cancer Trialists' Collaborative G, Davies C, Godwin J, Gray R, Clarke M, Cutter D, et al. Relevance of breast cancer hormone receptors and other factors to the efficacy of adjuvant tamoxifen: patient-level meta-analysis of randomised trials. Lancet 2011;378:771–84.

Published OnlineFirst June 26, 2017; DOI: 10.1158/0008-5472.CAN-17-0657

Cancer Research
The Journal of Cancer Research (1916–1930) | The American Journal of Cancer (1931–1940)

AACR American Association for Cancer Research

SPIN90 Depletion and Microtubule Acetylation Mediate Stromal Fibroblast Activation in Breast Cancer Progression

Eunae You, Yun Hyun Huh, Ahreum Kwon, et al.

Cancer Res 2017;77:4710-4722. Published OnlineFirst June 26, 2017.